

Noisy Cyclic Quantum Random Walk

G. Juárez Rangel^{1,*} and B. M. Rodríguez-Lara^{2,†}

¹*Tecnologico de Monterrey, Escuela de Ingeniería y Ciencias,
Ave. Eugenio Garza Sada 2501, Monterrey, N.L., Mexico, 64849*

²*Universidad Politécnica de Pachuca,
Carr. Pachuca-Cd. Sahagún Km.20,
Ex-Hda. Santa Bárbara, Zempoala, 43830, Hidalgo, Mexico*

(Dated: December 3, 2024)

Abstract

We explore static noise in a discrete quantum random walk over a homogeneous cyclic graph, focusing on the spectral and dynamical properties of the system. Using a three-parameter unitary coin, we control the spectral properties of the noiseless step operator on the unit circle in the complex plane. One parameter governs the probability amplitudes and induces two spectral bands, with a gap proportional to its value. The half-sum of the two phase parameters rotates the spectrum and induces twofold degeneracy under specific conditions. Degenerate spectra yield eigenstates with sinusoidal probability distributions, whereas non-degenerate spectra produce flat distributions. By using the eigenstate participation ratio, we predict the behavior of a walker under static phase noise in the coin and sites, showing a correlation between low participation ratios and localization, and high ratios with delocalization. Our results show that the average eigenstate participation ratio provides insights equivalent to computationally intensive mean squared displacement calculations. We observe a transition from super-diffusive to sub-diffusive behavior for uniformly distributed noise within the range $-\pi/3$ to $\pi/3$ and saturation of the mean square distance when the number of steps exceeds the graph size by an order of magnitude. Finally, we propose a quantum circuit implementation of our model.

* e-mail: a01570628@tec.mx

† e-mail: bmlara@upp.edu.mx, blas.rodriguez@gmail.com

I. INTRODUCTION

Anderson localization, first identified in disordered electronic systems, describes the inhibition of wave scattering caused by disorder in a medium [1–6]. This phenomenon arises from the interference of multiple propagation paths and occurs in various physical systems, including optical, acoustic, and quantum waves [7–11]. Random walks are an example of Anderson localization in the quantum domain, where the interplay between quantum coherence and randomness leads to diverse dynamical behaviors. These dynamics have potential applications in areas such as quantum transport modeling [12–15] and quantum computing [16, 17].

We are interested in Anderson localization in cyclic quantum random walks, where the walker is confined to a structure with periodic boundary conditions. These conditions introduce unique constraints, affecting the onset and nature of localization in the presence of disorder. Here, we systematically explore how disorder influences the localization properties, analyzing the probability distribution over time, the inverse participation ratio, and the effects of static noise in the coin and site phases. Our results reveal distinct dynamics of quantum localization in cyclic systems, offering insight into potential applications where generation and control of localized quantum states is crucial [18–28]. Additionally, we compare our findings with those in non-cyclic systems to highlight the distinct features of cyclic quantum walks. Our analysis shows that cyclic topology can either mitigate or intensify localization effects depending on the disorder characteristics and system parameters.

The article is structured as follows. In Section II, we present the theoretical implementation of the discrete-time quantum random walk on a cyclic graph with a parameterized coin and analyze its effect on the eigenvalues. In Section III, we investigate the effects of coin parameters on the eigenstates, probability distribution, participation ratio, degeneracy, and localization. In Section IV, we introduce static phase noise in the sites, optimizing the noise range to enhance localization and distinguishing between sub-diffusive, diffusive, and ballistic spread for both the Hadamard and symmetric coins. We propose an implementation of the cyclic quantum random walk on a gate-based quantum computer in Sec.V. We conclude in Section VI with a summary of our results and their implications.

II. QUANTUM RANDOM WALK IN A CYCLIC GRAPH

An ideal, lossless, discrete-time quantum random walk relies on two components, a coin and an adjoint pair of step operators [29]. The state of the coin defines the direction of the step. The step-coin operator produces a unitary process that preserves the total probability of the system in the ideal, lossless case.

We define a general unitary coin with three real parameters [4],

$$\hat{C}(\gamma, \theta, \phi) = \cos \gamma |0\rangle\langle 0| + e^{i\theta} \sin \gamma |0\rangle\langle 1| + e^{i\phi} \sin \gamma |1\rangle\langle 0| - e^{i(\theta+\phi)} \cos \gamma |1\rangle\langle 1|, \quad (1)$$

where the parameter $\gamma \in [0, \pi/2]$ controls the probability amplitudes between the basis states and modifies the hopping strength, while the parameters $\theta, \phi \in [0, 2\pi]$ control the coherence and interference in the quantum walk. This coin is non-Hermitian and its eigenstates and eigenvalues are complex,

$$\begin{aligned} |c_j\rangle &= \alpha_j |0\rangle + \sqrt{1 - |\alpha_j|^2} |1\rangle, \\ c_j &= s + (-1)^j \sqrt{e^{i(\theta+\phi)} + s^2}, \end{aligned} \quad (2)$$

with $s = \{[1 - e^{i(\theta+\phi)}] \cos \gamma\}/2$ and $\alpha_j = \tilde{\alpha}_j / \sqrt{4 + |\tilde{\alpha}_{1+(-1)^j}|^2}$, where $\tilde{\alpha}_j = 2(e^{-i\phi} c_j + e^{i\theta} \cos \gamma) \csc^{1-j} \gamma$ and $j = 0, 1$. For example, the parameter set $\{\gamma, \theta, \phi\} = \{\pi/4, 0, 0\}$ yields the Hadamard coin, which produces a balanced superposition of the walker position states. Applied to a localized initial state $|j\rangle|+\rangle$, the Hadamard coin tends to asymmetrically distribute the probability amplitude along the line [30, 31]. In contrast, the parameter set $\{\gamma, \theta, \phi\} = \{\pi/4, \pi/2, \pi/2\}$ yields the symmetric coin, which produces a balanced superposition of the walker's position. Applied to a localized initial state $|j\rangle|+\rangle$, this coin symmetrically distributes the probability amplitude equally along the line.

The step operator in the discrete cyclic quantum random walk,

$$\hat{S}_N = \left(\hat{V}_N \otimes \hat{P}_0 + \hat{V}_N^\dagger \otimes \hat{P}_1 \right) \left[\hat{1} \otimes \hat{C}(\gamma, \theta, \phi) \right], \quad (3)$$

is proportional to the clockwise and counter-clockwise step operators on the cyclic graph,

$$\begin{aligned} \hat{V}_N &= \sum_{j=1}^N |\text{mod}_N(j) + 1\rangle\langle j|, \\ \hat{V}_N^\dagger &= \sum_{j=1}^N |\text{mod}_N(j - 2) + 1\rangle\langle j|. \end{aligned} \quad (4)$$

where we used $\text{mod}_N(-1) = N - 1$. The step operators move the state of the system to the nearest neighbor in a clockwise or counter-clockwise direction, conditional on the state of the coin after the coin projector operator $\hat{P}_j = |j\rangle\langle j|$ acts on it. By moving into a reference frame rotating at the site frequency and using the quantum Fourier transform [32–34],

$$\hat{F}_N = \frac{1}{\sqrt{N}} \sum_{j,k=1}^N e^{i\frac{2\pi}{N}((j-1)(k-1))} |j\rangle\langle k|, \quad (5)$$

we diagonalize the step operators,

$$\begin{aligned} \hat{F}_N^\dagger \hat{V}_N \hat{F}_N &= \hat{\Lambda}_N, \\ \hat{F}_N^\dagger \hat{V}_N^\dagger \hat{F}_N &= \hat{\Lambda}_N^\dagger, \end{aligned} \quad (6)$$

in terms of the diagonal clock operator [35],

$$\hat{\Lambda}_N = \sum_{j=1}^N e^{-i\frac{2\pi}{N}(j-1)} |j\rangle\langle j|, \quad (7)$$

providing the eigenstates and eigenvalues [33],

$$\begin{aligned} |\lambda_k\rangle &= \hat{F}_N |k\rangle = \sum_{j=1}^N e^{i\frac{2\pi}{N}(j-1)(k-1)} |j\rangle, \\ \lambda_k &= e^{-i\frac{2\pi}{N}(k-1)}, \end{aligned} \quad (8)$$

distributed nonlinearly on a line with $k = 1, 2, \dots, N$. We now use the eigenstates of the coin and the step operators on the cyclic graph to build those of the discrete step operator,

$$\begin{aligned} |\zeta_k\rangle &= \cos \vartheta |\lambda_k, 0\rangle + e^{i\varphi_-} \sin \vartheta |\lambda_k, 1\rangle, \\ \zeta_k &= e^{-i\{\arcsin[\cos \gamma \sin \varphi_+] - \frac{\theta + \phi}{2}\}}, \end{aligned} \quad (9)$$

with real angles $\vartheta = -\arctan \left[\left(\cos \varphi_+ \pm \sqrt{\tan^2 \gamma + \cos^2 \varphi_+} \right) / \tan^2 \gamma \right]$ and $\varphi_{\pm} = 2\pi k/N \pm (\theta \pm \phi)/2$. The eigenvalues depend only on the half-sum of the two coin phases $(\theta + \phi)/2$ rather than their individual values. The argument of the eigenvalues, $\omega_k = \arg \zeta_k$, forms two bands $(\theta + \phi)/2 + \gamma \mp \pi/2 < \omega_k < (\theta + \phi)/2 - \gamma \pm \pi/2$, which close for $\gamma = 0$. In the complex plane, the ζ_k eigenvalues trace two $(\pi - 2\gamma)$ arcs of a unit circle, rotated by the half-sum of the coin phases relative to the real axis, Fig. 1.

Pairs of degenerate eigenvalues appear when the half-sum of the coin phases satisfies $(\theta + \phi)/2 = m\pi/N$ with $m = 0, 1, \dots, N - 1$. Otherwise, no spectral degeneracy exists. In the degenerate case, the probability distribution for the step eigenfunctions, after tracing out the coin, forms a sinusoidal pattern shape with maximum values of $2/N$, Fig. 2(a). In contrast, for the non-degenerate case, the distribution is flat with value $1/N$, Fig. 2(b).

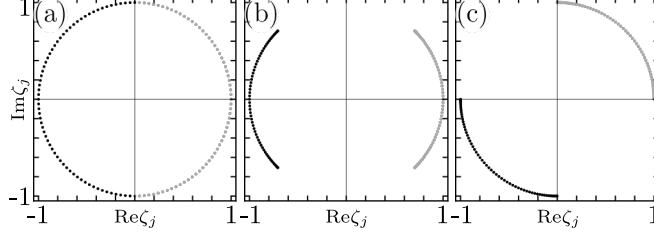


FIG. 1. Eigenvalues ζ_k in the complex plane for a cyclic graph with 128 identical sites and coin parameters $\{\gamma, (\theta + \phi)/2\}$ equal to (a) $\{0, 0\}$, (b) $\{\pi/4, 0\}$, and (c) $\{\pi/4, \pi/4\}$ with $\theta = \phi$.

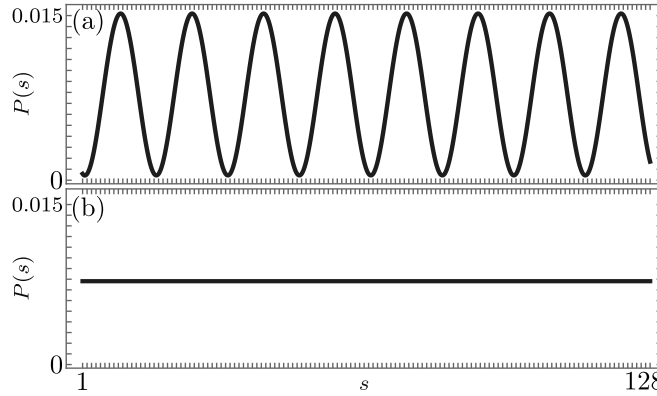


FIG. 2. Probability distribution on the cyclic graph sites $P(s)$, after tracing out the coin, for (a) the first eigenstate in the spectral degenerate case with $(\theta + \phi)/2 = m\pi/N$ and $m = 64$ and $N = 128$, and (b) the non-degenerate case with $(\theta + \phi)/2 = 5\pi/14$.

III. EFFECT OF THE COIN

To predict the behavior of the walker under a coin, we use the participation ratio,

$$\text{PR}(\zeta_j) = \frac{\left(\sum_{s=1}^N P(s)\right)^2}{\sum_{s=1}^N P^2(s)}, \quad (10)$$

defined in terms of the probability $P(s)$ of finding the step eigenstate $|\zeta_j\rangle$ at site s . The participation ratio ranges from one to the number of sites N . Low participation ratios indicate that most eigenstates are localized, causing the walker to concentrate around the initial position. High participation ratios suggest delocalization, where the walker is likely to spread out from the initial position.

Figure 3(a) shows the mean participation ratios for a coin with variable parameters γ and $\theta = \phi$ on a cyclic graph with $N = 32$ sites. We use an initial state localized at site $s_0 = 16$ to analyze the final state after $m = 1000$ steps. Quantum walks with a mean participation ratio

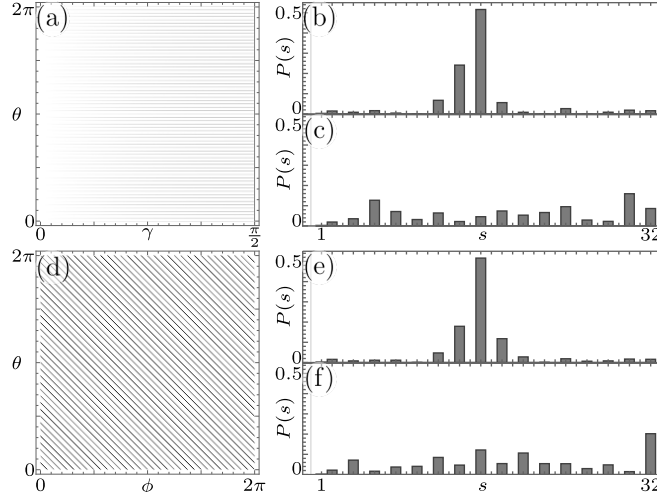


FIG. 3. Average participation ratio for the step eigenstates using a coin with (a) variable γ and $\theta = \phi$, and (d) fixed $\gamma = \pi/4$ with variable θ and ϕ . White corresponds to a PR equal to the size of the graph with $N = 32$. Final state probability distribution on the cyclic graph sites $P(s, m)$, after tracing out the coin, for $N = 32$, $m = 1000$, and coin parameters $\{\gamma, \theta, \phi\}$ producing localization, (b) $\{1/4, 5/32, 5/32\} \pi$ and (e) $\{1/4, 13/32, 17/32\}$, as well as delocalization, (c) $\{1/4, 5.5/32, 5.5/32\} \pi$ and (f) $\{1/4, 12/32, 17/32\} \pi$.

of 2.99 localize the walker, Fig. 3(b), while those with a mean participation ratio of 11.60 show delocalization, Fig. 3(c). Figures 3(d)-(f) present equivalent results for fixed $\gamma = \pi/4$ with variable θ and ϕ . In Fig. 3(b) and Fig. 3(e), we focus on the second minimum mean participation ratio, observing minimal spreading. Choosing the absolute minimum, $PR = 2$, would merely shift the initial state left and right of its original position. We optimized these results for cyclic graphs with 2^n sites, where $n = 5, 6, 7, 8$, consistently obtaining similar outcomes across each realization. However, visualizing the features becomes harder for larger graphs.

IV. STATIC NOISE IN THE SITES

Phase noise introduced in the cyclic graph step operators is equivalent to altering the self-energy terms in the continuous-time Hamiltonian. As a result, local perturbations can either enhance or inhibit interference, affecting localization and diffusion properties. We

consider a diagonal noise operator,

$$\hat{D}_{\text{noise}}(\varphi) = \sum_{s=1}^N e^{i\phi_s} |s\rangle\langle s|, \quad (11)$$

such that the noisy step operator is given by

$$\hat{S}_{\text{noise}}(\varphi) = \left(\hat{D}_{\text{noise}}(\varphi) \otimes \hat{1} \right) \hat{S}_N, \quad (12)$$

with real random phase noise in the range $\phi_s \in [-\varphi, \varphi]$. In the following, we optimize the random phase range to produce localization, using the participation ratio for the eigenvalues of the noisy step operator.

To quantify the spread of the walker at each step, we use the mean squared displacement on the cycle,

$$\Delta x^2(m) = \sum_{s=1}^N [\Delta x(m)]^2 P(s, m), \quad (13)$$

in terms of the probability $P(s, m)$ of finding the walker at site s after m steps, and the mean displacement,

$$\Delta x(m) = \min [|x(m) - x(0)|, N - |x(m) - x(0)|], \quad (14)$$

which is the minimum distance between the walker mean position at step m and its initial site. Here, the mean position of the walker on the cyclic graph is $x(m) = \langle \psi(m) | \hat{n} | \psi(m) \rangle$, where the site number operator is $\hat{n} = \sum_{s=1}^N s |s\rangle\langle s|$. Fitting the mean squared displacement to a power law,

$$\Delta x^2(m) \approx \alpha m^\beta, \quad (15)$$

allows us to quantify how fast the walker spreads over each step [13, 15, 36]. The exponent β helps us determine the walker spreading behavior. If $\beta = 2$, the walker spreads ballistically; $\beta = 1$ indicates diffusive spread, while $\beta \in (1, 2)$ corresponds to super-diffusive spread. For $\beta \in (0, 1)$, the walker exhibits sub-diffusive spread.

Figure 4 shows the mean squared displacement and probability distribution for a walker using a Hadamard coin on a cyclic graph with $N = 128$ sites. The cases with higher mean participation ratios, shown in Fig. 3(c) and Fig. 3(f), lead to ballistic and super-diffusive spread, Fig. 4(a) with $\beta = 1.996$ and Fig. 4(b) with $\beta = 1.794$. Figure 4(c) shows diffusive

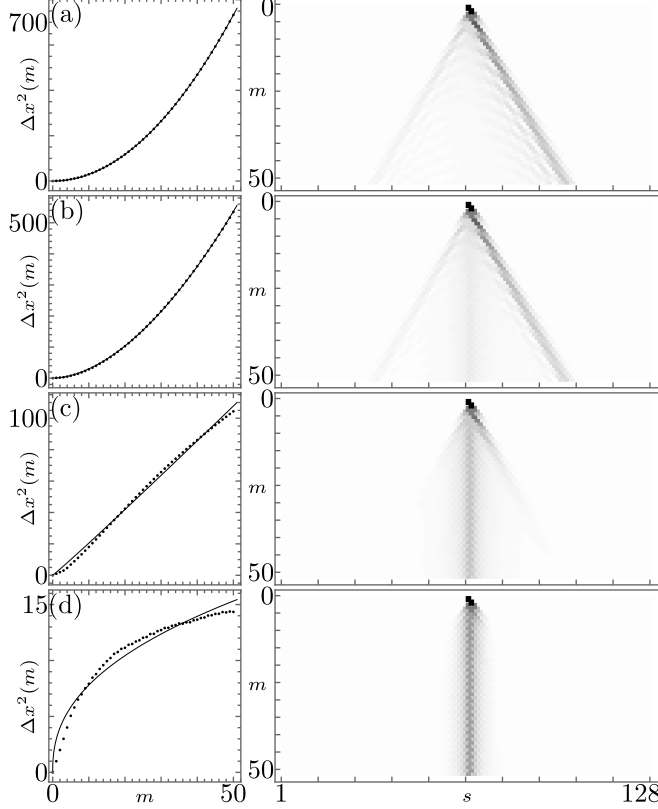


FIG. 4. Mean squared displacement $\Delta x^2(m)$ (left column) and probability of finding the walker at site s at step m , $P(s, m)$, for a graph with size $N = 128$ with coin parameters $\{\pi/4, 0, 0\}$ for noise levels ϕ_s , rate of spread α , and power law fit β . The values $\{\phi_s, \alpha, \beta\}$ are equal to (a) $\{0, 0.297, 1.996\}$, (b) $\{\pi/10, 0.480, 1.794\}$, (c) $\{\pi/3, 1.901, 1.032\}$, (d) $\{\pi, 2.973, 0.419\}$.

spread with $\beta = 1.032$. The cases with lower mean participation ratios, shown in Fig. 3(b) and Fig. 3(e), result in sub-diffusive spread, Fig. 4(d) with $\beta = 0.419$. A noise level of $\phi_s = \pi/3$ marks the threshold between sub-diffusive and super-diffusive spread.

Figure 5 shows the mean squared displacement and the probability distribution of the walker at each step of the evolution for a symmetric coin. The results of the symmetric coin are comparable to those observed with the Hadamard coin, except that the symmetric coin produces a symmetric probability at each step.

Figure 6 shows the mean square displacement over 1024 steps on a cyclic graph with $N = 128$ sites. In the ballistic and super-diffusive spread cases, the mean square displacement oscillates as the walker repeatedly reaches the opposite side of the graph. Each oscillation amplitude gradually decreases, indicating convergence, Fig.6(a) and Fig.6(b). In contrast, the diffusive and sub-diffusive cases rapidly converge to a constant mean square

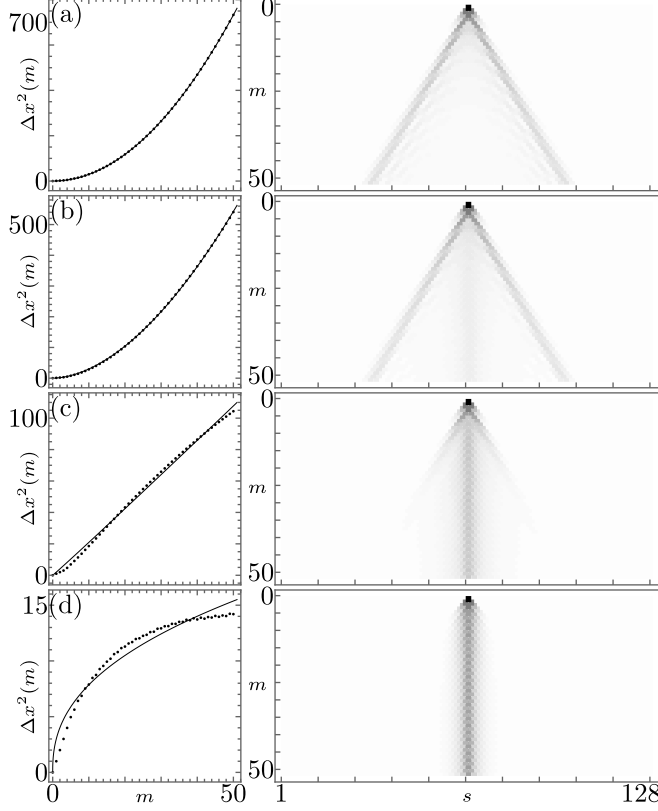


FIG. 5. Mean squared displacement $\Delta x^2(m)$ (left column) and probability of finding the walker at site s at step m , $P(s, m)$, for a graph with size $N = 128$ with coin parameters $\{\pi/4, \pi/2, \pi/2\}$ for noise levels ϕ_s , rate of spread α , and power law fit β . The values $\{\phi_s, \alpha, \beta\}$ are equal to (a) $\{0, 0.298, 1.996\}$, (b) $\{\pi/10, 0.475, 1.800\}$, (c) $\{\pi/3, 2.005, 1.019, \}$, (d) $\{\pi, 3.006, 0.417\}$.

displacement, Fig. 6(c) and Fig. 6(d), with no indication of completing a full cycle within the 1024 steps.

Figure 7 shows the participation ratio boxplot distribution and spread α at different noise levels for the Hadamard coin (left column) and the symmetric coin (right column). For both coins, we observe a direct relationship between the participation ratio and the spread α , with a minimum value at the maximum noise level $\phi_s = \pi$.

V. QUANTUM CIRCUIT IMPLEMENTATION

In gate-based quantum computing, a general unitary operator may be implemented using a sequence of three rotations, $\hat{R}_z(\alpha)\hat{R}_y(\theta)\hat{R}_z(\beta)$. We define rotations around the Pauli- j axis

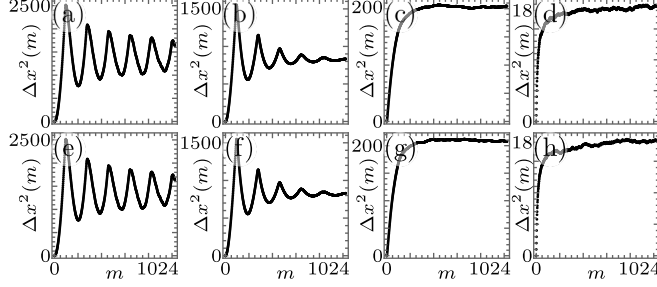


FIG. 6. Mean squared displacement $\Delta x^2(m)$ for 1024 steps with $N = 128$ and parameters identical to those in Fig. 4 for the Hadamard case (a) to (d) and 5 for the symmetric case (e) to (h).

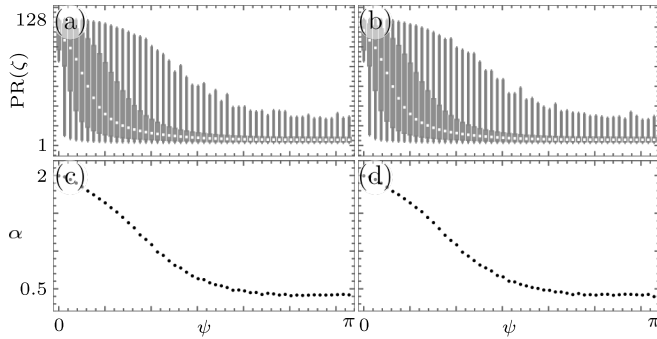


FIG. 7. Participation ratio boxplots (first row) depicting the distribution and rate of spread α for different noise levels ϕ_s with coin parameters $\{\pi/4, 0, 0\}$ (a), (c) and $\{\pi/4, \pi/2, \pi/2\}$ (b), (d).

as $\hat{R}_j(\vartheta) = \cos(\vartheta/2)\hat{1} + i \sin(\vartheta/2)\hat{\sigma}_j$ with $j = x, y, z$ [37]. Thus, the coin operator,

$$\hat{C}(\gamma, \theta, \phi) = \hat{R}_z(\phi)\hat{R}_y(2\gamma)\hat{R}_z(\theta + \pi), \quad (16)$$

may be implemented in such a quantum computer.

The step operator relies on the quantum Fourier transform (QFT), which scales quadratically with the number of qubits [37]. Figure 8 illustrates the QFT algorithm for n logical qubits. The QFT uses the phase gate $P_j = |0\rangle\langle 0| + |0\rangle\langle 1| + |1\rangle\langle 0| + e^{i\pi/2^j} |1\rangle\langle 1|$, with rotation angle $\pi/2^j$, to achieve the desired diagonalization.

The diagonal clockwise and counter-clockwise operators can be implemented using controlled phase gates. Figure 9 presents the corresponding circuits for $N = 2^n$ sites. These circuits exploit the additive property of phase gates, $P(\theta)P(\phi) = P(\theta + \phi)$, enabling efficient implementation of higher-order iterations.

We show an optimized step operator circuit in Fig. 10. This approach reduces the reliance on two-qubit gates, which are typically more error-prone, by leveraging the diagonal

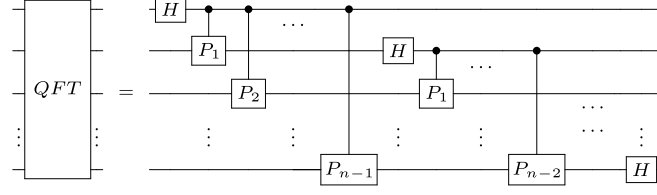


FIG. 8. Quantum Fourier transform (QFT) circuit for n logical qubits, where P_j is the phase gate with rotation angle $\pi/2^j$.

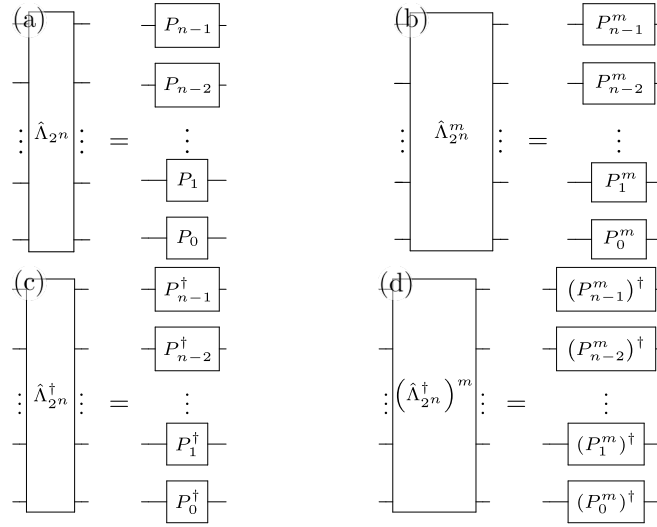


FIG. 9. Circuit implementations for the diagonal (a) clockwise and (c) counter-clockwise operators, and (b) and (d) their higher-order iterations, respectively. Here, P_j and P_j^m represent phase gates with rotation angles $\pi/2^j$ and $m\pi/2^j$, in that order.

representation of the clock operators.

For multiple-step implementations, the circuit in Fig. 11 implements repeated applications of the step operator. When introducing static noise into the sites, as described in Section IV, the noise operator must be incorporated into the Fourier basis. Figure 12 demonstrates this integration. While the Fourier-transformed noise operator can be computationally intensive, efficient decomposition can be left to a transpiler, such as in the Qiskit framework.

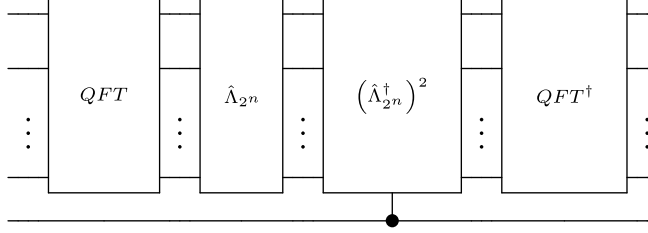


FIG. 10. Efficient step operator circuit for n logical qubits, incorporating diagonal clockwise and counter-clockwise operators with phase gates P_j .

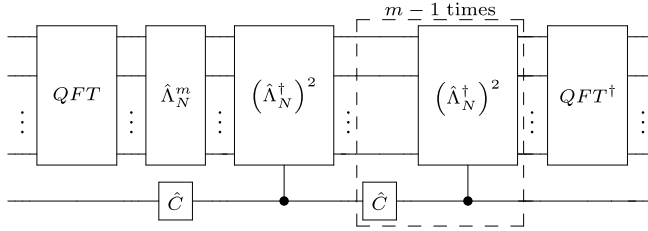


FIG. 11. Algorithm for performing multiple steps in the cyclic graph with coin operator \hat{C} .

VI. CONCLUSION

We investigated Anderson localization in cyclic quantum random walks, showing that the half-sum of the coin phases determines walker evolution in the absence of noise. Introducing static phase noise at the sites, uniformly distributed over the range $[-\phi_n, \phi_n]$, induces a transition in walker dynamics from super-diffusive behavior at $\phi_n = 0$ to sub-diffusive behavior at $\phi_n = \pi/3$. Maximum localization occurs for noise uniformly distributed over the range $[-\pi, \pi]$.

Our analysis of the mean squared displacement revealed oscillatory behavior in the super-diffusive and ballistic regimes, with eventual convergence. In contrast, sub-diffusive walkers exhibited exponential convergence. Furthermore, we showed that eigenstate statistics for

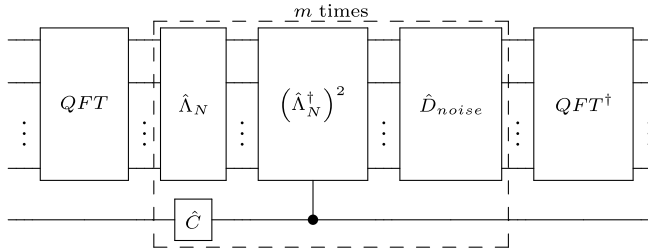


FIG. 12. Algorithm for performing multiple steps with static phase noise on the cyclic graph.

the noisy step operator offer an efficient method for predicting walker behavior, requiring significantly fewer computational resources compared to calculating the mean squared displacement across noisy realizations. Our approach could optimize the analysis of quantum systems and enhance the understanding of quantum transport in disordered environments.

Our findings hold promise for improving the robustness of quantum devices against noise. Future research could explore the effects of dynamical noise, providing deeper insights into the evolution of quantum walks under time-dependent perturbations and their implications for localization phenomena [18, 20–23, 26, 27].

FUNDING

Not Applicable

ACKNOWLEDGMENT

B. M. R. L. acknowledge fruitful discussion with Emiliano Etienne Iracheta.

DISCLOSURES

The authors declare no conflicts of interest.

DATA AVAILABILITY

Data underlying the results presented in this paper may be obtained from the authors upon reasonable request.

-
- [1] Y. Lahini, A. Avidan, F. Pozzi, M. Sorel, R. Morandotti, D. N. Christodoulides, and Y. Silberberg, Anderson localization and nonlinearity in one-dimensional disordered photonic lattices, *Phys. Rev. Lett.* **100**, 013906 (2008), arXiv:0704.3788 [quant-ph].

- [2] A. Crespi, R. Osellame, R. Ramponi, V. Giovannetti, R. Fazio, L. Sansoni, F. De Nicola, F. Sciarrino, and P. Mataloni, Anderson localization of entangled photons in an integrated quantum walk, *Nat. Photon.* **7**, 322 (2013), arXiv:1304.1012 [quant-ph].
- [3] M. Segev, Y. Silberberg, and D. N. Christodoulides, Anderson localization of light, *Nat. Photon.* **7**, 197 (2013).
- [4] I. Vakulchyk, M. V. Fistul, P. Qin, and S. Flach, Anderson localization in generalized discrete-time quantum walks, *Phys. Rev. B* **96**, 144204 (2017), arXiv:1708.08194 [quant-ph].
- [5] S. Weidemann, M. Kremer, S. Longhi, and A. Szameit, Coexistence of dynamical delocalization and spectral localization through stochastic dissipation, *Nat. Photon.* **15**, 576 (2021).
- [6] S. Longhi, Anderson localization in dissipative lattices, *Ann. Phys.* **535**, 2200658 (2023), arXiv:2304.07710 [quant-ph].
- [7] C. A. Condat and T. R. Kirkpatrick, Resonant scattering and Anderson localization of acoustic waves, *Phys. Rev. B* **36**, 6782 (1987).
- [8] R. L. Weaver, Anderson localization of ultrasound, *Wave Motion* **12**, 129 (1990).
- [9] J. Billy, V. Josse, Z. Zuo, A. Bernard, B. Hambrecht, P. Lugan, D. Clément, L. Sanchez-Palencia, P. Bouyer, and A. Aspect, Direct observation of Anderson localization of matter-waves in a controlled disorder, *Nature* **453**, 891 (2008), arXiv:0804.1621 [quant-ph].
- [10] M. Piraud, L. Sanchez-Palencia, and B. van Tiggelen, Anderson localization of matter waves in three-dimensional anisotropic disordered potentials, *Phys. Rev. A* **90**, 063639 (2014).
- [11] Y. Ye, M. Ke, J. Feng, M. Wang, C. Qiu, and Z. Liu, Transversal Anderson localization of sound in acoustic waveguide arrays, *J. Phys. Condens. Matter* **27**, 155402 (2015).
- [12] A. Schreiber, K. N. Cassemiro, V. Potoček, A. Gábris, I. Jex, and C. Silberhorn, Decoherence and disorder in quantum walks: from ballistic spread to localization, *Phys. Rev. Lett.* **106**, 180403 (2011), arXiv:1101.2638 [quant-ph].
- [13] F. Nosrati, A. Laneve, M. K. Shadfar, A. Gherardi, K. Mahdavi-pour, F. Pegoraro, P. Mataloni, and R. Lo Franco, Readout of quantum information spreading using a disordered quantum walk, *J. Opt. Soc. Am. B* **38**, 2570 (2021), arXiv:2010.10592 [quant-ph].
- [14] A. R. C. Buarque, F. S. Passos, W. S. Dias, and E. P. Raposo, Discrete-time quantum walk dispersion control through long-range correlations, *Phys. Rev. E* **107**, 064139 (2023), arXiv:2303.01608 [quant-ph].

- [15] G. R. M. de Almeida, N. Amaral, A. R. C. Buarque, and W. S. Dias, Noise correlations behind superdiffusive quantum walks, *Phys. Rev. E* **109**, 064151 (2024), arXiv:2207.13145 [quant-ph].
- [16] S. Derevyanko, Anderson localization of a one-dimensional quantum walker, *Sci. Rep.* **8**, 1795 (2018).
- [17] Q.-Q. Wang, X.-Y. Xu, W.-W. Pan, K. Sun, J.-S. Xu, G. Chen, Y.-J. Han, C.-F. Li, and G.-C. Guo, Dynamic-disorder-induced enhancement of entanglement in photonic quantum walks, *Optica* **5**, 1136 (2018), arXiv:1808.09298 [quant-ph].
- [18] P. Rebentrost, M. Mohseni, I. Kassal, S. Lloyd, and A. Aspuru-Guzik, Environment-assisted quantum transport, *New J. Phys.* **11**, 033003 (2009).
- [19] L. Sapienza, H. Thyrestrup, S. Stobbe, P. D. Garcia, S. Smolka, and P. Lodahl, Cavity quantum electrodynamics with Anderson-localized modes, *Science* **327**, 1352 (2010).
- [20] H. Obuse and N. Kawakami, Topological phases and delocalization of quantum walks in random environments, *Phys. Rev. B* **84**, 195139 (2011).
- [21] J. Asch, O. Bourget, and A. Joye, Dynamical localization of the Chalker-Coddington model far from transition, *J. Stat. Phys.* **147**, 194 (2012).
- [22] J. H. Bardarson, F. Pollmann, and J. E. Moore, Unbounded growth of entanglement in models of many-body localization, *Phys. Rev. Lett.* **109**, 017202 (2012).
- [23] K. Agarwal, S. Gopalakrishnan, M. Knap, M. Müller, and E. Demler, Anomalous diffusion and Griffiths effects near the many-body localization transition, *Phys. Rev. Lett.* **114**, 160401 (2015).
- [24] C. M. Chandrashekar and T. Busch, Localized quantum walks as secured quantum memory, *Europhys. Lett.* **110**, 10005 (2015).
- [25] J. M. Edge and J. K. Asboth, Localization, delocalization, and topological transitions in disordered two-dimensional quantum walks, *Phys. Rev. B* **91**, 104202 (2015).
- [26] Q.-Q. Wang, X.-Y. Xu, W.-W. Pan, K. Sun, J.-S. Xu, G. Chen, Y.-J. Han, C.-F. Li, and G.-C. Guo, Dynamic-disorder-induced enhancement of entanglement in photonic quantum walks, *Optica* **5**, 1136 (2018).
- [27] Q. Lin, T. Li, L. Xiao, and et al., Observation of non-Hermitian topological Anderson insulator in quantum dynamics, *Nat. Commun.* **13**, 3229 (2022).
- [28] S. Pu, G. J. Sreejith, and J. K. Jain, Anderson localization in the fractional quantum Hall effect, *Phys. Rev. Lett.* **128**, 116801 (2022).

- [29] T. A. Brun, H. A. Carteret, and A. Ambainis, Quantum random walks with decoherent coins, *Phys. Rev. A* **67**, 032304 (2003).
- [30] A. Nayak and A. Vishwanath, Quantum walk on the line (2012), arXiv:0010117 [quant-ph].
- [31] C. M. Chandrashekar, R. Srikanth, and S. Banerjee, Symmetries and noise in quantum walk, *Phys. Rev. A* **76**, 022316 (2007).
- [32] Y. S. Weinstein, M. A. Pravia, E. M. Fortunato, S. Lloyd, and D. G. Cory, Implementation of the quantum Fourier transform, *Phys. Rev. Lett.* **86**, 1889 (2001).
- [33] D. J. Nodal Stevens, B. Jaramillo Ávila, and B. M. Rodríguez-Lara, Necklaces of PT-symmetric dimers, *Photon. Res.* **6**, A31 (2018), arXiv:1709.00498 [quant-ph].
- [34] B. Jaramillo Ávila, J. Naya Hernández, S. M. Toxqui Rodríguez, and B. M. Rodríguez-Lara, Symmetric supermodes in cyclic multicore fibers, *OSA Continuum* **2**, 515 (2019).
- [35] J. Košík, V. Bužek, and M. Hillery, Quantum walks with random phase shifts, *Phys. Rev. A* **74**, 022310 (2006).
- [36] M. Sassetti, H. Schomerus, and U. Weiss, Subdiffusive and superdiffusive quantum transport and generalized duality, *Phys. Rev. B* **53**, R2914 (1996).
- [37] M. A. Nielsen and I. L. Chuang, *Quantum Computation and Quantum Information: 10th Anniversary Edition* (Cambridge University Press, 2010).